

Comparative study on phase transition behaviors of fractional molecular field theory and random-site Ising model

Ting-Yu Liu(刘婷玉), Wei Zhao(赵薇), Tao Wang(王涛), Xiao-Dong An(安小冬), Lai Wei(卫来), and Yi-Neng Huang(黄以能)

Citation: Chin. Phys. B, 2024, 33 (**3**): 036403. DOI: 10.1088/1674-1056/ad0cc7
Journal homepage: http://cpb.iphy.ac.cn; http://iopscience.iop.org/cpb

What follows is a list of articles you may be interested in

Spatial distribution order parameter prediction of collective system using graph network

Huimin Zhao(赵慧敏), Rui Wang(王瑞), Cai Zhao(赵偲), and Wen Zheng(郑文)
Chin. Phys. B, 2023, 32 (**5**): 056402. DOI: 10.1088/1674-1056/acb9fa

Stability of the topological quantum critical point between multi-Weyl semimetal and band insulator

Zhao-Kun Yang(杨兆昆), Jing-Rong Wang(王景荣), and Guo-Zhu Liu(刘国柱)
Chin. Phys. B, 2023, 32 (**5**): 056401. DOI: 10.1088/1674-1056/acbaf2

Learning physical states of bulk crystalline materials from atomic trajectories in molecular dynamics simulation

Tian-Shou Liang(梁添寿), Peng-Peng Shi(时朋朋), San-Qing Su(苏三庆), and Zhi Zeng(曾志)
Chin. Phys. B, 2022, 31 (**12**): 126402. DOI: 10.1088/1674-1056/ac98a4

Solid-to-molecular-orientational-hexatic melting induced by local environment determined defect proliferations

Zhanglin Hou(侯章林), Jieli Wang(王杰利), Ying Zeng(曾颖), Zhiyuan Zhao(赵志远), Xing Huang(黄兴), Kun Zhao(赵坤), and Fangfu Ye(叶方富)
Chin. Phys. B, 2022, 31 (**12**): 126401. DOI: 10.1088/1674-1056/ac8ce1

Solid-liquid transition induced by the anisotropic diffusion of colloidal particles

Fu-Jun Lin(蔺福军), Jing-Jing Liao(廖晶晶), Jian-Chun Wu(吴建春), and Bao-Quan Ai(艾保全)
Chin. Phys. B, 2022, 31 (**3**): 036401. DOI: 10.1088/1674-1056/ac1e19

Comparative study on phase transition behaviors of fractional molecular field theory and random-site Ising model

Ting-Yu Liu(刘婷玉)[1], Wei Zhao(赵薇)[1], Tao Wang(王涛)[1], Xiao-Dong An(安小冬)[1], Lai Wei(卫来)[1,†], and Yi-Neng Huang(黄以能)[1,2,‡]

[1] *Xinjiang Laboratory of Phase Transitions and Microstructures in Condensed Matters, College of Physical Science and Technology, Yili Normal University, Yili* 835000, *China*

[2] *National Laboratory of Solid State Microstructures, School of Physics, Nanjing University, Nanjing* 210008, *China*

(Received 18 August 2023; revised manuscript received 31 October 2023; accepted manuscript online 16 November 2023)

Fractional molecular field theory (FMFT) is a phenomenological theory that describes phase transitions in crystals with randomly distributed components, such as the relaxor-ferroelectrics and spin glasses. In order to verify the feasibility of this theory, this paper fits it to the Monte Carlo simulations of specific heat and susceptibility versus temperature of two-dimensional (2D) random-site Ising model (2D-RSIM). The results indicate that the FMFT deviates from the 2D-RSIM significantly. The main reason for the deviation is that the 2D-RSIM is a typical system of component random distribution, where the real order parameter is spatially heterogeneous and has no symmetry of space translation, but the basic assumption of FMFT means that the parameter is spatially uniform and has symmetry of space translation.

Keywords: phase transition, molecular field theory, Ising model, Monte Carlo

PACS: 64.60.Bd, 64.60.De, 77.80.Jk, 75.50.Lk **DOI:** 10.1088/1674-1056/ad0cc7

1. Introduction

Although there is some overlap in time, the theoretical explorations of the phase transition for ferroelectricity, ferromagnetism, etc. can be divided into two main stages. The first one (approximately 1908–1975) mainly focuses on macroscopic crystalline materials with uniform distribution of components (commonly referred to as homogeneous systems). Specifically, all elements (atoms, molecules, ions, etc.) have the periodicity in spatial distribution on the crystal lattice or symmetry of space translation, such as barium titanate[1,2] and potassium dihydrogen phosphate[3,4] of ferroelectrics, as well as iron and nickel[5,6] of ferromagnets. While the second stage (approximately 1954 to now) mainly focuses on the macroscopic crystalline materials of component heterogeneous distribution, specifically the random distribution of some kinds of elements on the crystal lattice (no symmetry of space translation), also known as the crystals of component random distribution, such as lead magnesium niobate[7–10] and barium zirconate titanate[11,12] of ferroelectrics (including relaxor-ferroelectrics and dipole glasses), as well as gold iron,[13] bismuth manganese scandate[14,15] of ferromagnets (including relaxor-ferromagnets and spin glasses), etc.[16–20]

After the first stage of researches, a gradually mature theoretical system for ferroelectric and ferromagnetic phase transitions in the crystals of uniformly distributed components has been established, including the phenomenological theories (Weiss molecular field theory,[21,22] Landau theory,[23] Devonshire theory,[24–26] etc.), and the microscopic models (Ising model,[27] Heisenberg model,[28] etc.) as well as the corresponding solution methods (Weiss mean field,[22] Bethe mean field,[29] matrix transformation,[30,31] Wilson momentum space renormalization group theory,[32] and Kadanoff position space renormalization group theory[33]).

Although some research progress of the crystals of component random distribution has been made in the second stage, there are still many unsolved problems. For example, in terms of microscopic model and solution method studies, random-site Ising model,[34,35] random-site Heisenberg model,[35] random-bond Ising (Edwards–Anderson) model,[35,36] random-bond Heisenberg model,[35] etc. have been proposed, but the advances in solving the models are extremely limited so far, for these models have no spatial translation symmetry, the renormalization group method, which is extremely effective for systems with component uniform distribution, is no longer applicable. At present, there are mainly the replica method to the random-bond Ising model[35,36] and spin-string mean-field method to the random-site Ising model[37] (it seems that this method is also effective for the random-site Heisenberg model). As for the researches on phenomenological theory, Kuehn and Kliem[38] proposed the fractional molecular field theory (FMFT), which seems to be related to the mesoscopic fractal structures[39,40] formed by the random distribution of components on crystal lattice. However, the effectiveness of this theory still needs to be further verified.

To solve this problem, this paper first briefly introduces

†Corresponding author. E-mail: lweiphy@sina.com
‡Corresponding author. E-mail: ynhuang@nju.edu.cn

© 2024 Chinese Physical Society and IOP Publishing Ltd

FMFT, then uses Monte Carlo method (MC)[41–43] to simulate the phase transition behaviors (specific heat and susceptibility versus temperature) of the two-dimensional (2D) random-site Ising model (2D-RSIM),[35,37] and detailed comparative studies of the behaviors of FMFT and 2D-RSIM are conducted.

2. Fractional molecular field theory

The basic assumptions of FMFT[38] are made below. (i) Like Weiss molecular field theory, any pseudospin (magnetic or electric dipole) in a crystal of component random distribution is approximated as an Ising spin ($\sigma = 1$ or -1), and (ii) the interaction energy between an Ising spin in the crystal and the other is $-J_{\rm F}\eta^{\gamma}\sigma$, where $\eta \equiv \langle\sigma\rangle$ is the thermodynamic statistical average of σ such as blow, $J_{\rm F}$ the interaction energy constant independent of temperature (T), and γ a fractional factor ($0 < \gamma \leq 1$) also independent of T, which is the reason why it is called FMFT. Therefore, in an external static field B (when B denotes magnetic field or electric field, then corresponding dipole is magnetic or electric dipole, respectively) along the Ising spin direction, the Hamiltonian ($\mathcal{H}_{\rm F}$) of an Ising spin in the crystal is

$$\mathcal{H}_{\rm F} = -\left(J_{\rm F}\eta^{\gamma} + \mu B\right)\sigma, \tag{1}$$

where μ is the dipole moment of the magnetic or electric dipole. Corresponding to $\mathcal{H}_{\rm F}$, the partition function ($Z_{\rm F}$) of the spin is

$$Z_{\rm F} \equiv \sum_{\sigma=1,-1} \exp\left(-\frac{H_{\rm F}}{k_{\rm B}T}\right) = 2\cosh\left(\frac{J_{\rm F}\eta^{\gamma}+\mu B}{k_{\rm B}T}\right). \tag{2}$$

When the crystal is at thermal equilibrium,

$$\begin{aligned}\eta &\equiv \frac{1}{Z_{\rm F}}\sum_{\sigma=1,-1}\sigma\exp\left(-\frac{H_{\rm F}}{k_{\rm B}T}\right)\\ &= \tanh\left(\frac{J_{\rm F}\eta^{\gamma}+\mu B}{k_{\rm B}T}\right).\end{aligned} \tag{3}$$

The order parameter ($\eta_{\rm s}$), i.e., reduced spontaneous magnetization or polarization of the crystal is obtained from Eq. (3), specifically, it is expressed as

$$\eta_{\rm s} = \tanh\left(\frac{J_{\rm F}\eta_{\rm s}^{\gamma}}{k_{\rm B}T}\right). \tag{4}$$

The internal energy (U) and specific heat (C) per spin without external field are given below:

$$\begin{aligned}U &\equiv \lim_{B\to 0}\frac{1}{2Z_{\rm F}}\sum_{\sigma=1,-1}H_{\rm F}\exp\left(-\frac{H_{\rm F}}{k_{\rm B}T}\right)\\ &= -\frac{J_{\rm F}\eta_{\rm s}^{\gamma}}{2}\tanh\left(\frac{J_{\rm F}\eta_{\rm s}^{\gamma}}{k_{\rm B}T}\right),\end{aligned} \tag{5}$$

$$C \equiv \frac{\partial U}{\partial T}. \tag{6}$$

In addition, according to Eq. (3), the static susceptibility (χ) per spin is

$$\chi \equiv \mu_0\mu\lim_{B\to 0}\frac{\partial\eta}{\partial B} = \mu_0\mu^2\frac{1-\eta_{\rm s}^2}{k_{\rm B}T - J_{\rm F}\gamma\eta^{\gamma-1}\left(1-\eta_{\rm s}^2\right)}, \tag{7}$$

where μ_0 is the vacuum permeability.

Figure 1 shows the curves of calculated C, χ, and $\eta_{\rm s}$ versus reduced temperature ($k_{\rm B}T/J_{\rm F}$) by FMFT (Eqs. (4)–(7)). For $\gamma = 1$, FMFT is simplified into Weiss molecular field theory.[21] At this point, C and χ exhibit sharp λ-type peaks, and the peak temperature ($T_{\rm c}^{\rm h}$) of the C peak is the same as that of the χ peak ($T_{\rm c}^{\rm s}$). $\eta_{\rm s}$ first slowly, then rapidly decreases with T increasing, and to 0 at $T_{\rm c}^{\rm h}$ and $T_{\rm c}^{\rm s}$. As γ decreases: (i) the C peak and χ peak become diffuse and gradually flatten; (ii) $T_{\rm c}^{\rm h}$ moves to low temperature, but $T_{\rm c}^{\rm s}$ first to high temperature and then to low one (Fig. 3), and (iii) $\eta_{\rm s}$ first slowly, then rapidly, and slowly decreases again as T rises.

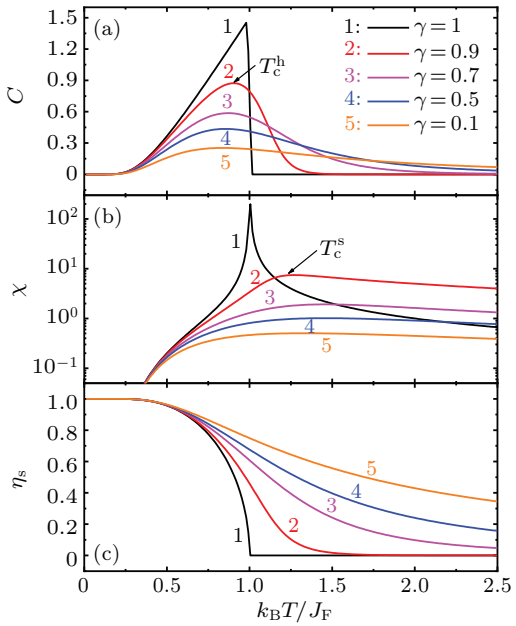


Fig. 1. Curves of specific heat (C), susceptibility (χ), and order parameter ($\eta_{\rm s}$) per spin of fractional molecular field theory versus reduced temperature ($k_{\rm B}T/J_{\rm F}$) for $\gamma = 1$, 0.9, 0.7, 0.5, and 0.1, respectively.

Mathematically, $\gamma = 1$ is for the case of the second-order phase transition, and $\eta_{\rm s} = 0$ above the transition temperature. But when $\gamma < 1$, $\eta_{\rm s} \neq 0$ at high temperatures because $\eta_{\rm s}^{\gamma} > \eta_{\rm s}$, i.e., $\eta_{\rm s}$ expands to a high temperature region and exhibits a diffuse phase transition. Physically, $\gamma < 1$ corresponds to the fractional feedback of the molecular field, i.e., percolation effect, phenomenologically, which leads to the dispersion of the transition process.

3. 2D random-site Ising model and Monte Carlo simulation

The Hamiltonian ($\mathcal{H}$) of 2D-RSIM[35,37] is

$$\mathcal{H} = \mathcal{H}_0 - \mu B\lim_{n\to\infty}\sum_{i=1}^{n}\sum_{j=1}^{n}\sigma_{i,j}r_{i,j}^{\phi}, \tag{8a}$$

$$\mathcal{H}_0 = -J \lim_{n\to\infty}\left[\sum_{i=1}^{n-1}\sum_{j=1}^{n}\sigma_{i,j}\sigma_{i+1,j}r_{i,j}^{\phi}r_{i+1,j}^{\phi} + \sum_{i=1}^{n}\sum_{j=1}^{n-1}\sigma_{i,j}\sigma_{i,j+1}r_{i,j}^{\phi}r_{i,j+1}^{\phi}\right], \tag{8b}$$

where $\sigma_{i,j}$ represents the Ising spin on the i and j lattice points in the 2D square lattice, and $\sigma_{i,j}=1$ or -1; J is the interaction energy constant between the nearest-neighboring spins; ϕ ($0<\phi\leq 1$) is the spin concentration, i.e., the concentration of spin vacancies ($\sigma_{i,j}=0$) $1-\phi$; $r_{i,j}^{\phi}$ denotes a random function that describes the spin-site-distribution ($r_{i,j}^{\phi}=1$ for $r<\phi$ and $r_{i,j}^{\phi}=0$ for $r\geq\phi$, where r is a random number in a range between 0 and 1); n is the number of lattice points along the crystal axis ($n\to\infty$ describes the thermodynamic limit). In fact, $\mathcal{H}$ is the energy of the spin–orientation–configuration in the model system where the spin has a specific site distribution and take a value of 1 or -1.

In addition, the above spin system is in a heat bath of T with which energy can be exchanged, that is, the spin system and the heat bath combine to form a canonical ensemble.[35,37]

When the model system is at thermal equilibrium, based on Boltzmann–Gibbs statistics,[35] the average C, $\eta_{\rm s}$, and χ per spin are

$$C \equiv \frac{\partial U}{\partial T} = \frac{1}{k_{\rm B}T^2}\frac{1}{\phi}\lim_{B\to 0}\lim_{n\to\infty}\frac{\overline{\mathcal{H}^2}-\overline{\mathcal{H}}^2}{n^2}, \tag{9a}$$

$$\eta_{\rm s} = \frac{1}{\phi}\lim_{B\to 0}\lim_{n\to\infty}\frac{\overline{\varsigma}}{n^2}, \tag{9b}$$

$$\chi \equiv \mu_0\mu\lim_{B\to 0}\frac{\partial\eta}{\partial B} = \frac{\mu_0\mu^2}{k_{\rm B}T}\frac{1}{\phi}\lim_{B\to 0}\lim_{n\to\infty}\frac{\overline{\varsigma^2}-\overline{\varsigma}^2}{n^2}, \tag{9c}$$

where the energy average ($\overline{\mathcal{H}}$), energy squared average ($\overline{\mathcal{H}^2}$), total spin average ($\overline{\varsigma}$), and total spin squared average ($\overline{\varsigma^2}$) of the system are

$$\overline{\mathcal{H}} \equiv \frac{1}{Z}\sum_{\{\sigma\}}\mathcal{H}\,{\rm e}^{-\beta\mathcal{H}}, \tag{10a}$$

$$\overline{\mathcal{H}^2} \equiv \frac{1}{Z}\sum_{\{\sigma\}}\mathcal{H}^2\,{\rm e}^{-\beta\mathcal{H}}, \tag{10b}$$

$$\overline{\varsigma} \equiv \frac{1}{Z}\sum_{\{\sigma\}}\sum_{i,j=1}^{n}\sigma_{i,j}r_{i,j}^{\phi}\exp(-\beta\mathcal{H}), \tag{10c}$$

$$\overline{\varsigma^2} \equiv \frac{1}{Z}\sum_{\{\sigma\}}\left[\sum_{i,j=1}^{n}\sigma_{i,j}r_{i,j}^{\phi}\right]^2\exp(-\beta\mathcal{H}), \tag{10d}$$

where Z is the partition function corresponding to $\mathcal{H}$ and expressed as

$$Z \equiv \sum_{\{\sigma\}}\exp(-\beta\mathcal{H}), \tag{11}$$

where $\{\sigma\}$ represents the sum of all spin states ($\sigma_{i,j}=1$ or -1) in the system, and $\beta\equiv(k_{\rm B}T)^{-1}$.

According to Eqs. (9)–(10), in principle, C, χ, and $\eta_{\rm s}$ of 2D-RSIM at thermal equilibrium can be calculated exactly, but as mentioned above, their exact solutions have not been obtained so far. The simulations of C, χ, and $\eta_{\rm s}$ of 2D-RSIM by using the MC method and the simulated results are provided in the following.

According to Boltzmann–Gibbs statistics, when calculating the thermodynamic parameters such as C and χ of the Ising model, a certain spin–orientation configuration of the model is defined as a spin–orientation system, and the set of all such different systems is called a spin–orientation ensemble (SOE). Therefore, in the calculation of these parameters, only SOE needs to be statistically averaged.[30] However, when calculating the parameters of random-site Ising model, it is also necessary to consider the site distribution $r_{i,j}^{\phi}$ of spins on lattice, i.e., not only does it require statistical averaging of the SOE with a certain site distribution, but also statistical averaging of spin–site distribution.[35,37] Here, the set of SOEs with all spin–site distribution is collectively referred to as spin–site superensemble. The specific MC simulation[43] of this superensemble is as follows.

(I) Selection of simulated lattice size

Because a macroscopic crystal contains a huge spin number, it can often be regarded as an infinite system. However, when simulating it, only a finite system can be selected due to limitations in computer memory and runtime. This work simulates a 2D-RSIM with a selected spin number of 200^2, i.e., $n=200/\sqrt{\phi}$. Due to the inevitable existence of boundaries in a finite system, we select a free boundary condition, which means that there is no interaction between the spins at the boundaries and the outside of the simulated system.

(II) Simulation of random spin distribution on a lattice

A random number r between 0 and 1 is generated corresponding to each lattice point. If $r\leq\phi$, a spin is placed at the point, i.e., $r_{i,j}^{\phi}=1$, and if $r>\phi$, no spin or a spin vacancy at the point, i.e., $r_{i,j}^{\phi}=0$.

(III) Processing of $B\to 0$

In this work, we take $B=0$, and due to the possible multi-domain formation in the simulation system,[31,43] the obtained $\eta_{\rm s}$ may not be reliable, so it is not given here.

(IV) Simulation of spin flipping

Herein we select the Glauber dynamics of the spin flip,[35,37,43,44] i.e., the transformations in different spin–orientation systems are caused by the single spin flipping, and the probability of achieving a flip from $\sigma_{i,j}$ to $-\sigma_{i,j}$ during each attempt is

$$p = \frac{\exp\left(\dfrac{\sigma_{i,j}F_{i,j}}{k_{\rm B}T}\right)}{\exp\left(\dfrac{\sigma_{i,j}F_{i,j}}{k_{\rm B}T}\right)+\exp\left(-\dfrac{\sigma_{i,j}F_{i,j}}{k_{\rm B}T}\right)}, \tag{12a}$$

where $F_{i,j}$ is the local field of $\sigma_{i,j}$, and

$$F_{i,j} \equiv J\big(\sigma_{i-1,j}r^{\phi}_{i-1,j}+\sigma_{i+1,j}r^{\phi}_{i+1,j} +\sigma_{i,j-1}r^{\phi}_{i,j-1}+\sigma_{i,j+1}r^{\phi}_{i,j+1}\big). \tag{12b}$$

The simulation process of a single spin flip involves a random number r between 0 and 1, which is generated by the random number function, and the spin flips for $p > r$ but not for $p \le r$. Here, we choose that all spins in the system successively attempt to flip once as one MC step.

(V) Simulation of thermal equilibrium of spin–orientation ensemble

In this paper we select all spins up ($\sigma_{i,j} = 1$) in a spin–orientation system as the initial state. After each MC step, a new spin–orientation system is generally obtained. Corresponding to the k-th MC step, the energy ($\mathcal{H}^l_k$) and total spin (ς^l_k) of the simulated k-th spin–orientation system are

$$\mathcal{H}^l_k = -J\left[\sum_{i=1}^{n-1}\sum_{j=1}^{n}\sigma^{k,l}_{i,j}\sigma^{k,l}_{i+1,j}r^{\phi,l}_{i,j}r^{\phi,l}_{i+1,j} +\sum_{i=1}^{n}\sum_{j=1}^{n-1}\sigma^{k,l}_{i,j}\sigma^{k,l}_{i,j+1}r^{\phi,l}_{i,j}r^{\phi,l}_{i,j+1}\right], \tag{13a}$$

$$\varsigma^l_k = \sum_{i=1}^{n}\sum_{j=1}^{n}\sigma^{k,l}_{i,j}r^{\phi,l}_{i,j}, \tag{13b}$$

where l is the serial number of an SOE in the spin–site superensemble, $\sigma^{k,l}_{i,j}$ is the spin value at the lattice point of i and j in the k-th system of the l-th SOE.

Because a canonical ensemble is simulated in this work,[35,43] we choose $\mathcal{H}^l_k$ that varies with k as the criterion parameter of thermal equilibrium. Specifically, if the average value of $\mathcal{H}^l_k$ within a certain step interval is nearly unchanged with k, it is considered that the simulated system tends to thermal equilibrium.

Due to the fact that this work focuses on simulating the phase transition characteristics of 2D-RSIM, i.e., the temperature range studied is near the phase transition, and the simulation results show that after $k > 10^3$, the systems substantially tend to thermal equilibrium. Here, the MC step ($k_{\rm E}$) selected to reach thermal equilibrium is 30000, and the total MC step ($k_{\rm F}$) is 35000.

(VI) Simulation of thermodynamic parameters of spin–orientation ensemble

The basic assumption of MC simulation[35,43] is that the average energy ($\overline{\mathcal{H}}_l$), average energy square ($\overline{\mathcal{H}^2}_l$), average total spin ($\overline{\varsigma}_l$), and average total spin square ($\overline{\varsigma^2}_l$) of the l-th SOE can be approximated by the following equations:

$$\overline{\mathcal{H}}_l \approx \frac{1}{k_{\rm F}-k_{\rm E}+1}\sum_{k=k_{\rm E}}^{k_{\rm F}}\mathcal{H}^l_k, \tag{14a}$$

$$\overline{\mathcal{H}^2}_l \approx \frac{1}{k_{\rm F}-k_{\rm E}+1}\sum_{k=k_{\rm E}}^{k_{\rm F}}\mathcal{H}^{l^2}_k, \tag{14b}$$

$$\overline{\varsigma}_l \approx \frac{1}{k_{\rm F}-k_{\rm E}+1}\sum_{k=k_{\rm E}}^{k_{\rm F}}\varsigma^l_k, \tag{14c}$$

$$\overline{\varsigma^2}_l \approx \frac{1}{k_{\rm F}-k_{\rm E}+1}\sum_{k=k_{\rm E}}^{k_{\rm F}}\varsigma^{l^2}_k. \tag{14d}$$

(VII) Selection of SOE number in spin–site superensemble

Due to the spin–site distribution, the number (n_l) of SOEs in the spin–site superensemble is $C^{\phi n^2}_{n^2}$, where $C^{\cdots}_{\cdots}$ is the number of combinations. Considering the limitations of computer runtime, we choose $n_l = 10$ for simulation.

(VIII) Simulation of thermodynamic parameters of superensemble

The basic assumption of MC simulation[35,43] is that $\overline{\mathcal{H}}$, $\overline{\mathcal{H}^2}$, $\overline{\varsigma}$, and $\overline{\varsigma^2}$ of the spin–site superensemble can be approximated by the following equations:

$$\overline{\mathcal{H}} \approx \frac{1}{n_l}\sum_{l=1}^{n_l}\overline{\mathcal{H}}_l, \tag{15a}$$

$$\overline{\mathcal{H}^2} \approx \frac{1}{n_l}\sum_{l=1}^{n_l}\overline{\mathcal{H}^2}_l, \tag{15b}$$

$$\overline{\varsigma} \approx \frac{1}{n_l}\sum_{l=1}^{n_l}\overline{\varsigma}_l, \tag{15c}$$

$$\overline{\varsigma^2} \approx \frac{1}{n_l}\sum_{l=1}^{n_l}\overline{\varsigma^2}_l. \tag{15d}$$

Based on the simulation results of Eq. (15), and according to Eq. (9), C and χ of 2D-RSIM can be simulated, and the results are shown in Fig. 2.

4. Comparison of FMFT predictions and 2D-RSIM simulations

The γ and $J_{\rm F}$ in FMFT are the parameters which affect the peak height and peak position of C and χ, respectively. Among them, γ controls the height of the peak: the larger the value of γ, the higher the peak height is; while $J_{\rm F}$ regulates the peak position: the larger the value of $J_{\rm F}$, the higher the peak position towards high temperature is.

Figure 2 shows the fitting of C and χ versus T by FMFT to the simulation results of 2D-RSIM,with black squares representing the case of $\phi = 0.9$ and $n = 211$; red circles are the case of $\phi = 0.8$ and $n = 224$; blue diamonds are the case of $\phi = 0.7$ and $n = 239$, magenta stars are the case of $\phi = 0.6$ and $n = 258$). Figures 2(a) and 2(b) represent the preferential fits to C (Fig. 2(a)) of 2D-RSIM by FMFT, with black solid line denoting the case of $\gamma = 0.99$ and $J_{\rm F}/J = 2.00$; red solid line the case of $\gamma = 0.86$ and $J_{\rm F}/J = 1.80$; blue solid line the case of $\gamma = 0.70$ and $J_{\rm F}/J = 1.65$; magenta solid line the case of $\gamma = 0.55$ and $J_{\rm F}/J = 1.50$), and then χ is calculated by the corresponding γ and $J_{\rm F}/J$ (Fig. 2(b)). While figures 2(c) and 2(d) are those of preferential fits to χ, with black solid line referring to the case of $\gamma = 0.995$ and $J_{\rm F}/J = 1.90$; red solid line

the case of $\gamma = 0.993$ and $J_F/J = 1.58$; blue solid line the case of $\gamma = 0.980$ and $J_F/J = 1.20$; magenta solid line the case of $\gamma = 0.950$ and $J_F/J = 0.75$).

Figure 2(a) shows that FMFT performs poorly in fitting the C peak shape of 2D-RSIM with $\phi = 0.9$, but as ϕ decreases, the fitting becomes better and better. However, for the same values of γ and J_F, the calculated χ has significant deviations from the 2D-RSIM simulation results, including significantly higher T_c^s, different peak shapes, and 1–2 orders of magnitude smaller peak heights (Fig. 2(b)).

Figure 2(d) shows that although FMFT fits well to T_c^s and the χ peak height of 2D-RSIM, it has a poor fit to the peak shape, mainly manifested by large deviations from the high-temperature side. For the same values of γ and J_F, the calculated C not only lowers T_c^h and increases peak height significantly, but there is also a noticeable difference in peak shape (Fig. 2(c)).

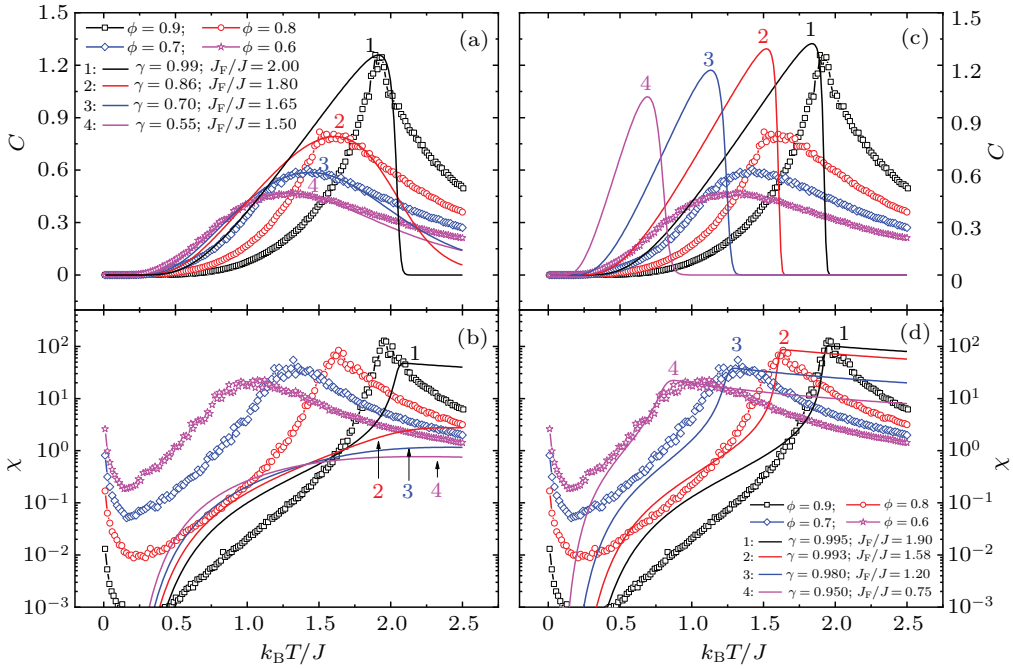


Fig. 2. Fitting to simulated specific heat (C) and susceptibility (χ) results (symbol) of the 2D random-site Ising model versus temperature (T) by the fractional molecular field theory (solid line), where panels (a) and (b) represent the preferential fits to C, while panels (c) and (d) to χ.

Figure 3(a) indicates that T_c^h and T_c^s are equal for $\gamma = 1$, and with decreasing γ: (i) T_c^h decreases rapidly in the range of 1–0.9, and then slowly in 0.9–0.1, and (ii) T_c^s rapidly increases to its maximum between 1 and 0.6, and then slowly decreases in the range of 0.6–0.1, but keeps higher than that for $\gamma = 1$. In Fig. 3(b), it can be seen that when ϕ is greater than 0.8, T_c^h almost coincides with T_c^s of 2D-RSIM and decreases with ϕ decreasing. However, there is a bifurcation between T_c^h and T_c^s when ϕ is less than 0.8, and comparing with T_c^s, the decreasing trend of T_c^h is slower with ϕ decreasing.

When comparing T_c^h and T_c^s of FMFT and 2D-RSIM, it is usually thought that $\gamma = 1$ in FMFT corresponds to $\phi = 1$ in 2D-RSIM. Some results can be seen from Fig. 3 as follows. (i) T_c^h of 2D-RSIM first decreases rapidly and then slowly with ϕ decreasing, which is consistent with the change trend of FMFT; (ii) T_c^s of 2D-RSIM goes down with ϕ decreasing and is always lower than that for $\phi = 1$, while T_c^s of FMFT shows a trend of first increasing and then decreasing with γ decreasing, and is always greater than that for $\gamma = 1$. This is one of the main differences between FMFT and 2D-RSIM.

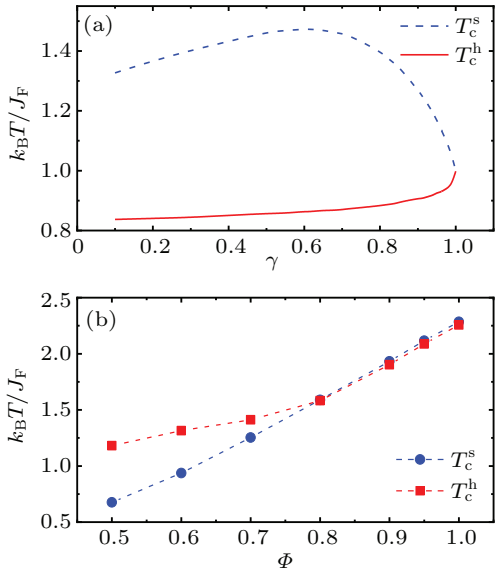


Fig. 3. (a) Peak temperatures of specific heat (T_c^h) and susceptibility (T_c^s) versus fractional factor (γ) of fractional molecular field theory. (b) T_c^h and T_c^s versus spin concentration (ϕ) for 2D random-site Ising model.

The main reason for the significant deviations of FMFT from 2D-RSIM (Figs. 2 and 3) is as follows. (i) Because 2D-

RSIM is a typical component non-uniform system,[34,35,37] its real order parameter must be spatially heterogeneous[39,40,45] and has no symmetry of space translation. However, the basic assumption of FMFT (Eq. (1)) "eliminates" this spatial heterogeneity and restores the symmetry of space translation; and (ii) due to the random distribution of spins in the RSIM model, the interaction experienced by each spin is stochastic. However, FMFT averages this interaction, ignoring the corresponding random fluctuations. This is also the main reason why the introduction of local order parameter,[37] i.e., the spatial non-uniformity considered, can achieve more accurate descriptions to the random-site Ising model.

5. Summary

This article compares the phase transition behaviors of FMFT with the simulation results of 2D-RSIM. The findings are as follows. (i) When FMFT is used to preferentially fit C of 2D-RSIM, the corresponding χ has significant deviations, manifested as significantly higher T_c^s, different peak shapes, and 1–2 orders of magnitude smaller peak heights. (ii) When fitting χ preferentially, the high-temperature side of χ deviates significantly, and the corresponding deviation of C is greater, including obviously lower T_c^h, higher peak height, and significant differences in peak shape. (iii) Especially when γ decreases from 1 to 0, the predicted T_c^s of FMFT is always higher than that for $\gamma = 1$, which has opposite tendency to the results of 2D-RSIM (where T_c^s always decreases with ϕ decreasing). In summary, the fitting accuracy of FMFT to 2D-RSIM is relatively low, and the main reason is that 2D-RSIM is a typical component non-uniform system, its real order parameter is spatially heterogeneous and has no symmetry of space translation, but the basic assumption of FMFT (Eq. (1)) smooths out the spatial heterogeneity and restores the symmetry of space translation.

Data availability statement

The data that support the findings of this study are openly available in Science Data Bank at https://doi.org/10.57760/sciencedb.13807.

Acknowledgements

The authors thank Prof. Zhang Li-Li and Zhou Heng-Wei for inspiring discussion.

Project supported by the Open Project of the Key Laboratory of Xinjiang Uygur Autonomous Region, China (Grant No. 2021D04015) and the Yili Kazakh Autonomous Prefecture Science and Technology Program Project, China (Grant No. YZ2022B021).

References

[1] Megaw H D 1947 *Proc. Roy. Soc. London A* **189** 261
[2] Vonhippel A 1950 *Rev. Mod. Phys.* **22** 221
[3] Stephenson C C and Hooley J G 1944 *J. Am. Chem. Soc.* **66** 1397
[4] Mason W P 1946 *Phys. Rev.* **69** 173
[5] Pallister P R 1949 *J. Iron Steel Inst.* **161** 87
[6] Ododo J C 1977 *Sol. Stat. Comm.* **22** 585
[7] Bovtun V, Veljko S, Kamba S, Petzelt J, Vakhrushev S, Yakymenko Y, Brinkman K and Setter N 2006 *J. Eur. Cera. Soc.* **26** 2867
[8] Zhao X, Qu W, Tan X, Bokov A A and Ye Z G 2007 *Phys. Rev. B* **75** 104106
[9] Tachibana M, Sasame K, Kawaji H, Atake T and Takayama-Muromachi E 2009 *Phys. Rev. B* **80** 94115
[10] Smolenskii G A and Rozgachev K I 1954 *Z. Tekhn. Fiziki* **24** 1751
[11] Maiti T, Guo R and Bhalla A S 2008 *J. Am. Cera. Soc.* **91** 1769
[12] Petzelt J, Bovtun V, Nuzhnyy D, Kempa M, Savinov M, Pasciak M, Kamba S, Canu G and Buscaglia V 2021 *Phys. Stat. Sol. B* **258** 210025910
[13] Coles B R, Sarkissian B V B and Taylor R H 1978 *Phil. Mag. B* **37** 489
[14] Belik A A, Yokosawa T, Kimoto K, Matsui Y and and Takayama-Muromachi E 2007 *Chem. Mat.* **19** 1679
[15] Belik A A and Takayama-Muromachi E. 2008 *J. Phys.: Condens. Matter* **20** 025211
[16] Qian X, Han D, Zheng L, Chen J, Tyagi M, Li Q, Du F, Zheng S, Huang X, Zhang S, Shi J, Huang H, Shi X, Chen J, Qin, H, Bernholc J, Chen X, Chen L Q, Hong L and Zhang Q M 2021 *Nature* **600** 664
[17] Huang H, Zhang G, Ma X, Liang D, Wang J, Liu Y, Wang Q and Chen L Q 2018 *J. Am. Cera. Soc.* **101** 1566
[18] Gao R, Shi X, Wang J, Zhang G and Huang H 2021 *Adv. Fun. Mater.* **31** 2104393
[19] Gao R, Shi X, Wang J and Huang H 2022 *J. Am. Cera. Soc.* **105** 3689
[20] Liu N, Huang S, Li J Q and Liang J Q 2019 *Acta Phys. Sin.* **68** 193701 (in Chinese)
[21] Weiss P 1908 *Phys. Z* **9** 358
[22] Yin H, Zhou H and Huang Y 2019 *Chin. Phys. Lett.* **36** 070501
[23] Landau L 1936 *Nature* **138** 840
[24] Devonshire A F 1949 *Phil. Mag.* **40** 1040
[25] Devonshire A F 1951 *Phil. Mag.* **42** 1065
[26] Devonshire A F 1954 *Adv. Phys.* **3** 85
[27] Ising E 1925 *Z. Phys.* **31** 253
[28] Heisenberg W 1928 *Z. Phys.* **49** 619
[29] Bethe H A 1938 *J. Appl. Phys.* **9** 244
[30] Onsager L 1944 *Phys. Rev.* **65** 117
[31] Yang C N 1952 *Phys. Rev.* **85** 808
[32] Wilson K G and Fisher M E 1972 *Phys. Rev. Lett.* **28** 240
[33] Kadanoff L P 1975 *Phys. Rev. Lett.* **34** 1005
[34] Klein M W and Brout R 1963 *Phys. Rev.* **132** 2412
[35] Binder K and Young A P 1986 *Rev. Mod. Phys.* **58** 801
[36] Edwards S F and Anderson P W 1975 *J. Phys. F* **5** 965
[37] Zhang L L and Huang Y N 2020 *Sci. Rep.* **10** 5060
[38] Kuehn M and Kliem H 2010 *Ferroelectrics* **400** 52
[39] Shvartsman V V, Kleemann W, Lukasiewicz T and Dec J 2008 *Phys. Rev. B* **77** 054105
[40] Shvartsman V V, Dkhil B and Kholkin A L 2013 *Ann. Rev. Mat. Res.* **43** 423
[41] Tian Z N, Ouyang X P, Chen W, Wang X M, Deng N, Liu W B and Tian Y J 2019 *Acta Phys. Sin.* **68** 232901 (in Chinese)
[42] Chen Z, Zhao Z J, Lü Z L, Li J H and Pan D M 2019 *Acta Phys. Sin.* **68** 215201 (in Chinese)
[43] Kurt B 1986 *Monte Carlo methods in statistical physics* (Heidelberg: Springer Berlin) p. 4
[44] Glauber R J 1963 *J. Math. Phys.* **4** 294
[45] Shvartsman V V and Lupascu D C 2012 *J. Am. Cera. Soc.* **95** 1